



# A Dynamo-based Forecast of Solar Cycle 25

Francois Labonville<sup>1</sup> · Paul Charbonneau<sup>1</sup> ·  
Alexandre Lemerle<sup>2</sup>

Received: 29 January 2019 / Accepted: 14 June 2019 / Published online: 26 June 2019  
© Springer Nature B.V. 2019

**Abstract** We present a data-driven version of the solar cycle model of Lemerle and Charbonneau (*Astrophys. J.* **834**, 133; 2017), which we use to forecast properties of the upcoming sunspot Cycle 25. The two free parameters of the model are fixed by requiring the model to reproduce Cycle 24 upon being driven by active region data for Cycle 23. Our forecasting model incorporates self-consistently the expected fluctuations associated with stochastic variations in properties of emerging active regions, most notably the scatter in the tilt angle of the line segment joining the opposite polarity foci of bipolar magnetic regions, as embodied in Joy's law. By carrying out ensemble forecasts with statistically independent realizations of active region parameters, we can produce error bars that capture the impact of this physical source of fluctuations. We forecast a smoothed monthly international sunspot number (version 2.0) peaking at  $89^{+29}_{-14}$  in year  $2025.3^{+0.89}_{-1.05}$ , with a 6 month onset delay in the northern hemisphere, but a peak amplitude 20% higher than in the southern hemisphere.

**Keywords** Solar cycle, models · Solar cycle, observations · Magnetic fields, photosphere

## 1. Introduction

The solar cycle is the magnetic pulse modulating the frequency of all geoeffective eruptive phenomena. The large-scale magnetic field it generates is also carried by the solar wind, and structures the interplanetary environment well beyond Earth's orbit. Interesting in and of itself because of what it can teach us about the mode of operation of the solar dynamo,

---

✉ P. Charbonneau  
[paulchar@astro.umontreal.ca](mailto:paulchar@astro.umontreal.ca)

F. Labonville  
[francois@astro.umontreal.ca](mailto:francois@astro.umontreal.ca)

A. Lemerle  
[lemerle@astro.umontreal.ca](mailto:lemerle@astro.umontreal.ca)

<sup>1</sup> Département de Physique, Université de Montréal, Montréal, QC, Canada

<sup>2</sup> Collège Bois-de-Boulogne, Montréal, QC, Canada

decadal-scale forecast of the properties of upcoming cycles is also useful and desired information in the planning of space missions and, more generally, in the mitigation of deleterious space weather events.

A wide variety of mathematical and physical forecasting schemes have been designed towards the prediction of solar cycles (see, *e.g.*, Petrovay, 2010; Pesnell, 2012, and the references therein). To date the most successful class of forecasting schemes remains that based on the use of the surface solar dipole moment at activity minimum as a precursor for the amplitude of the upcoming cycle (Schatten *et al.*, 1978; Svalgaard, Cliver, and Kamide, 2005). The logic behind these schemes is entirely in line with a dynamo-based explanation of the solar cycle: shearing of a pre-existing dipole by the solar internal differential rotation generates the large-scale internal toroidal magnetic flux system from which magnetic flux ropes will form, destabilize due to magnetic buoyancy, and eventually emerge at the photosphere as bipolar sunspot groups.

Given this success it is natural that further improvements were sought through the design of forecasting schemes based explicitly on data-driven dynamo models. The two Cycle 24 forecasts produced in this manner by Dikpati, de Toma, and Gilman (2006) and Choudhuri, Chatterjee, and Jiang (2007) are particularly interesting in this respect; working with similar dynamo models, these two groups of authors arrived at Cycle 24 forecasts standing at opposite ends of the very wide range of forecasts for Cycle 24 (see Figure 3 in Pesnell, 2012). It is now understood that these discrepant forecasts were dependent on the manner in which data was assimilated into the model. Specifically, data driving of the model must retain, in one form or another, information regarding the scatter in active region properties, most importantly the distribution of tilt angles embodied in Joy's law, as this is increasingly recognized as a primary source of cycle-to-cycle variability (Dasi-Espuig *et al.*, 2010; Muñoz-Jaramillo *et al.*, 2013; Cameron *et al.*, 2014; Nagy *et al.*, 2017; Whitbread, Yeates, and Muñoz-Jaramillo, 2018, and the references therein). Tilt fluctuation was indeed incorporated, albeit indirectly, in the Cycle 24 forecast of Choudhuri, Chatterjee, and Jiang (2007), *via* their resetting procedure for the surface dipole at solar minimum; whereas Dikpati, de Toma, and Gilman (2006) assimilated active regions areas without consideration of their tilt pattern, leading to a Cycle 24 forecast largely off the mark.

This paper presents a Cycle 25 prediction obtained using the  $2 \times 2D$  dynamo model of Lemerle and Charbonneau (2017), based on the injection of Cycle 23 and 24 active region data into its surface module. Section 2 gives an overview of the model, reviews some of its most salient features for solar cycle prediction, and describes the manner in which it was modified to accept observed active regions as surface input. Section 3 describes the validation procedure of the prediction scheme, and Section 4 its forecast for Cycle 25. Section 5 offers a comparison of our Cycle 25 forecast to other forecasts recently published, and Section 6 closes the paper with a critical discussion of the potential systematic errors associated with known shortcomings of our dynamo model.

## 2. A Data-driven Dynamo Model

The assimilation of magnetographic and/or active emergence data into a dynamo model for the purpose of cycle forecast requires a detailed longitude/latitude representation of the solar photosphere. This was one of the motivations underlying the design and development of the Lemerle and Charbonneau (2017) solar cycle model (hereafter LC17; see also Lemerle, Charbonneau, and Carignan-Dugas 2015). The LC17 model is based on the coupling of a

conventional 2D (meridional plane) mean-field-like flux transport dynamo (the FTD module), to an equally conventional 2D (latitude–longitude) surface magnetic flux transport simulation (the SFT module). The FTD module provides the synthetic active region emergences driving the SFT module, while the latter provides the upper boundary condition that effectively acts as a poloidal source term in the FTD module, in the spirit of the Babcock–Leighton mechanism of poloidal field regeneration through the decay of active regions (see, *e.g.*, Charbonneau, 2014; Karak *et al.*, 2014, and the references therein). Both FTD and STF modules are kinematic, in the sense that all flow fields are time-independent and set *a priori* using analytical expressions reproducing surface measurements and helioseismic inferences. The mean magnetic cycle period is then set primarily by the adopted meridional flow speed, as with other kinematic FTD-type solar cycle models (see, *e.g.*, Dikpati and Charbonneau, 1999; Yeates, Nandy, and Mackay, 2008).

A key component of the LC17 dynamo model is the “emergence function” setting the probability of active region emergence in the SFT module in terms of the internal magnetic field strength and spatial distribution within the FTD module. The form of this function is set based on stability calculations carried out in the thin flux tube approximation (see LC17, Section 3.5). An emerging bipolar active region must also be assigned a flux value, pole separation, and tilt angle of the line joining the two members with respect to the E-W direction (as embodied by Joy’s law). These are all extracted from statistical distributions constructed using the database assembled by Wang and Sheeley (1989) for Solar Cycle 21 (see Lemerle, Charbonneau, and Carignan-Dugas, 2015, appendix). The observed scatter of tilt angles about the mean defined by Joy’s law turns out to be the primary source of stochasticity in the regeneration of the surface dipole (see LC17, Section 4.1; also Nagy *et al.* 2017), and thus of the simulated magnetic cycles in this dynamo model (on this point see also Cameron *et al.*, 2014). Both the amplitude and duration of individual cycles are strongly affected by these stochastic fluctuations in tilt angles (see Figures 8e and 9 in LC17), because of their strong impact on the strength of the surface dipole, and on the timing of its polarity inversions (see also Nagy *et al.*, 2017). Also important from the forecasting point of view, solar cycle simulations carried out with the LC17 model reproduce the observed correlation between the intensity of the surface dipole at activity minimum, and the amplitude of the subsequent magnetic cycle (see LC17, Figure 8f). Magnetically-mediated quenching of the mean tilt defined by Joy’s law is the only amplitude-limiting nonlinearity included in the model.

The emergence algorithm also includes a lower threshold on the internal toroidal field strength, as suggested by calculation of the stability and buoyant rise of toroidal magnetic flux ropes in the thin flux tube approximation (Schüssler *et al.*, 1994; Fan, 2009, and the references therein). The presence of this lower threshold ( $B^*$ ) implies that the resulting dynamo is not self-excited. However, once this threshold is exceeded, the growth rate of the dynamo is determined by the imposed proportionality factor ( $K$ ) setting the linear relationship between the probability of emergence in the SFT module and value of the emergence function at the same latitude. This quantity  $K$  acts as the dynamo number for the model, in the sense that it must exceed a critical value to yield sustained dynamo action; beyond this critical value,  $K$  sets the linear growth rate of the dynamo, and in the statistically stationary regime the cycle amplitude increases with increasing values of  $K$ . In what follows, the two parameters  $B^*$  and  $K$  will be the primary adjustable parameters for calibrating our prediction scheme on Cycle 24. The other model parameters are kept fixed at their values obtained in LC17 through a formal optimization procedure based on a genetic algorithm, minimizing the differences between synthetic and observed sunspot butterfly diagrams for Cycle 21.

The LC17 dynamo model is readily turned into a data-driven simulation by replacing the emergence algorithm with insertion of emerging active regions, with locations and physical characteristics inferred from magnetographic observations. Towards this end we used the database of bipolar magnetic regions determined from NSO synoptic Carrington maps, downloaded from the solar dynamo dataverse<sup>1</sup> maintained by A. Muñoz-Jaramillo (see also Yeates, Mackay, and van Ballegooijen, 2007). This database covers Carrington rotation 1911 to 2196 inclusive, corresponding to dates ranging from 29 June 1996 to 5 November 2017. The procedure used to construct the database from magnetograms is described in Section 4 of Yeates, Mackay, and van Ballegooijen (2007). The simulation thus embodies two distinct modes of operation: a “data-driven mode”, using the active region database to insert active regions in the SFT module; and a “dynamo mode”, using the emergence function protocol described previously. A forecast is produced by running the simulation in data-driven mode until some set date, and switching to dynamo mode to generate an ensemble of simulations with statistically independent realizations of active regions emergences. The forecast proper is then constructed from the statistical characterization of this ensemble.

Because it spans four centuries, the international sunspot number record (hereafter ISSN; see Clette *et al.*, 2014) remains the time series of choice to characterize the solar cycle and its fluctuations. Consequently, forecasts of upcoming solar cycles are most often expressed in terms of the sunspot number. Whether running the LC17 model in data-driven or dynamo modes, it is straightforward to calculate a time series unsigned surface magnetic flux  $\Phi(t)$  associated with emerging bipolar magnetic regions. The translation from unsigned surface magnetic flux to predicted ISSN is based on a linear fit between these two quantities, as extracted from the Cycle 23–24 database, and the ISSN (Version 2) as distributed by SILSO/SIDC<sup>2</sup> (see Clette and Lefèvre, 2016). Towards this end we use the 13-month smoothed monthly ISSN, and force the fit through (0, 0). This results in the linear relationship:

$$\text{ISSN} = 0.67 \times \frac{\Phi}{10^{21}} \text{ Mx} \quad [\text{Cycles } 23 + 24]. \quad (1)$$

Nonlinear or polynomial fits return relationships that hardly differ from the above linear relationship over the unsigned flux and ISSN ranges spanned by the data, motivating the use of Equation 1 to convert unsigned flux to ISSN. In applying this relationship to convert our time series of simulated surface magnetic flux for Cycle 25 into an ISSN forecast, we are assuming statistical stationarity in the relationship between ISSN and surface flux.

### 3. Calibration and Validation: Cycle 24

The aim is thus to initialize the dynamo model by assimilating active region emergence data into the model over Cycles 23 and 24, and then predict Cycle 25 by ensemble simulations running in dynamo mode. This requires setting an initial condition at the onset of Cycle 23, as well as adjusting (within their error bounds) some model parameters, most notably the dynamo number, which in the LC17 models sets the emergence probability per time step as a function of the internal toroidal field strength.

<sup>1</sup>This database is available at <https://dataverse.harvard.edu/dataverse/solardynamo>. The version used in the present work was downloaded in June 2018.

<sup>2</sup>These data are available at [www.sidc.be/silso/datafiles](http://www.sidc.be/silso/datafiles).

Starting with a pure dipole initial condition, we run the model in data-driven mode over the Cycle 23 portion of the active region database. In the spirit of data assimilation, we adjust the strength of this initial dipole so as to reproduce the observed dipole moment at the end of Cycle 23. We then use the resulting surface and internal magnetic field distribution as initial condition for simulating Cycle 24, and adjust the dynamo number  $K$  and emergence threshold parameter ( $B^*$  in Equation 10 of LC17) so as to reproduce as best as possible the time series of unsigned magnetic flux in active regions across Cycle 24, as well as the observed dipole strength on 5 November 2017, in the late descending phase of Cycle 24,  $\approx 2.0$  G. The synthetic butterfly diagrams are used as an additional discriminant, solutions producing emergence of active regions at high-latitude being excluded from the set of acceptable Cycle 24 solutions even if they show a good fit to the observed dipole moment and unsigned flux time series.

Assessing goodness of fit between our simulated Cycle 24 with the unsigned flux time series from the Yeates, Mackay, and van Ballegoijen (2007) database relies on an ensemble of 100 simulations of Cycle 24. Each ensemble member draws parameters of emerging active regions (flux, tilt, pole separation, etc.) from the same empirical statistical distributions, but does so using distinct random number streams. Goodness of fit is measured *via* a collective  $\chi^2$  between all ensemble members and the target unsigned flux time series.

Our best parameter set is  $K = 1.7$  and  $B_0 = 20$  G, and leads to the solution displayed on Figure 1. Here the model is run in data-driven mode until 12 June 2009 (thick vertical line), and switched to dynamo mode thereafter. The solid black line is the Cycle 24 target time series, and each member of the 100-member ensemble is plotted as a semi-transparent gray line. The thick black dashed line is a representative run, specifically that whose peak value is the median in the distribution of peak values for the 100-member ensemble. All time series plotted pertain to the 13-month smoothed time series of monthly-averaged surface unsigned magnetic flux values, in units of  $10^{21}$  Mx.

The time series of unsigned surface magnetic flux from the Yeates, Mackay, and van Ballegoijen (2007) database (thick solid line) is reproduced reasonably well, but there is also strong variability across ensemble members; this is a direct reflection of the impact of stochasticity in emerging active region properties, most importantly the scatter of tilt angles about Joy's law.

Examination of the axial dipole time series on the bottom panel of Figure 1 indicates a surface dipole in the late descending phase of Cycle 24 that is significantly stronger than observed, by almost a factor of two. This has no direct impact on the emerging magnetic flux, which is set by the internal magnetic field having built up during Cycle 23. Therefore this discrepancy is not a cause for concern from the point of view of fitting the emerging flux time series for Cycle 24. The real Cycle 24 dipole represents one instances of possible Cycle 24 realizations, which are strongly affected by the specificities of emerging active region properties (on this point see also Jiang, Cameron, and Schüssler, 2014; Nagy *et al.*, 2017).

#### 4. Forecast of Cycle 25

With the emergence threshold  $B^*$  and dynamo number  $K$  set by the reproduction of Cycle 24, we can now drive the dynamo with active region data for Cycles 23 and 24, up to 5 November 2017, and thereafter switch to dynamo mode to produce an ensemble of 100 forecasts for Cycle 25, each using a distinct stochastic realization of active region emergences. Figure 2 now shows the results of this exercise, in a format similar to Figure 1.

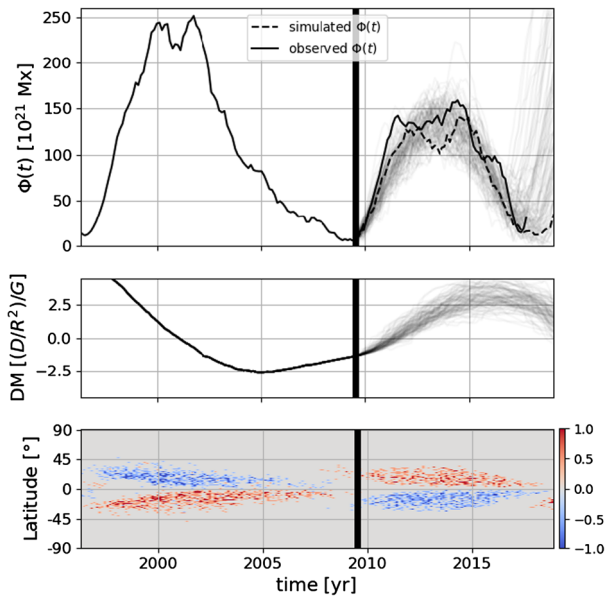


**Figure 1** Reproduction of Cycle 24 after data-driving over Cycle 23. On the *top panel*, the *thick dashed line* is the 13-month smoothed monthly unsigned surface magnetic flux time series for the solution whose peak value ranks as the median of the ranked peak values for the 100-member ensemble. The other individual ensemble members are plotted as semi-transparent *gray lines*. The *solid line* is the time series of surface magnetic flux directly constructed from the Yeates, Mackay, and van Ballegooijen (2007) database. In the *middle panel*, we plot the time series of the surface dipole moment for all 100 members of our ensemble. The *bottom panel* shows a time-latitude “butterfly diagram” of emerging active regions for the median-peak ensemble member (*dashed line on top panel*). All solutions use an emergence threshold  $B^* = 20$  and dynamo number  $K = 1.7$ , fluctuations being entirely due to stochasticity in emerging active region properties (see text).

The semi-transparent gray lines on Figure 2 are again the 13-month smoothed unsigned surface magnetic flux time series for our 100 ensemble members, and the thick dashed line is the member ranked as the median for the peak value of the unsigned surface magnetic flux reached at any time in the course of the cycle. Note also how the surface dipole strength in the late descending phase of Cycle 24 (1.7 G) is now much closer to the observed value ( $\approx 2.0$  G, from Wilcox Solar Observatory data<sup>3</sup>) than in the case of the simulated Cycle 24 on Figure 1. This confirms that the active regions having contributed most importantly to the polar field buildup in the descending phase of Cycle 24 are present in the Yeates, Mackay, and van Ballegooijen (2007) database.

Our ensemble of simulated Cycle 25 points towards a cycle slightly weaker than Cycle 24, of relatively short duration, and with a long rising phase peaking in the first half of 2025. Because our forecast model incorporates a full latitude–longitude representation of the solar photosphere, it is also possible to forecast quantities often not accessible to schemes operating only on global time series, most notably related to hemispheric asymmetries. Figure 3 replots the Cycle 25 forecast for surface magnetic flux, taken from Figure 2, this time separating the contributions of the two solar hemispheres. Once again significant variability is present across ensemble members, but overall amplitudes are lower by some 20 percent in

<sup>3</sup>These data are available at <http://wso.stanford.edu>.

**Figure 2** Similar to Figure 1 but now driving the model with active region data for Cycle 23 and 24, and switching to dynamo mode on 5 November 2017 (*thick vertical line*). The format of the three panels is the same as on Figure 1.

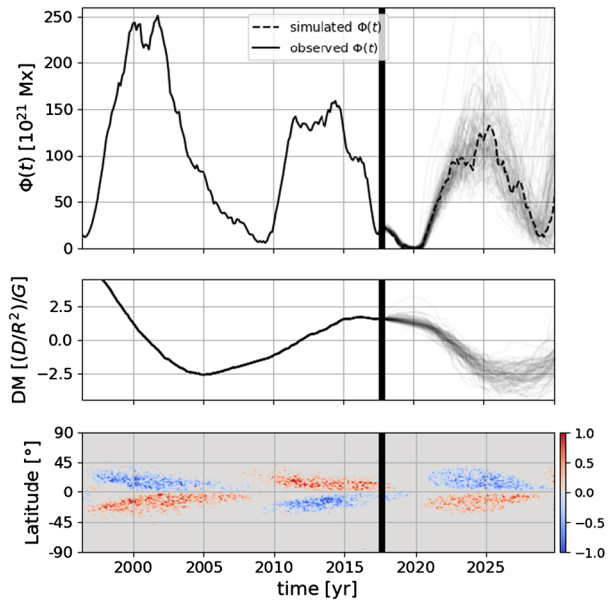
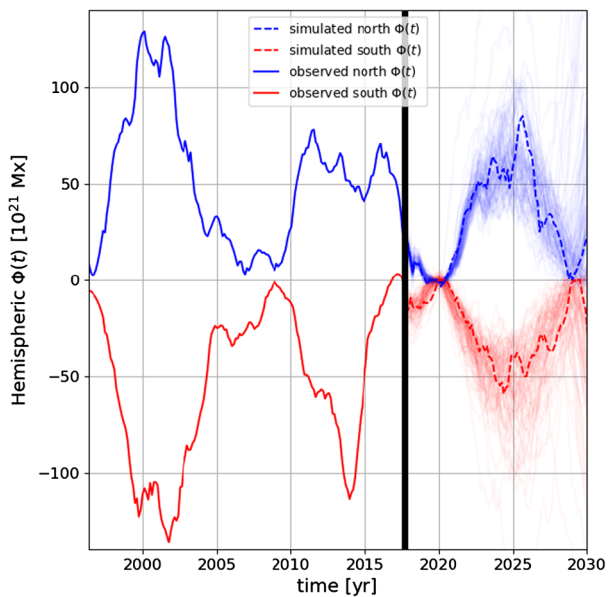


**Figure 3** Hemispheric unsigned flux time series corresponding to the ensemble forecast of Figure 2. The southern hemisphere time series is assigned negative values strictly for plotting purposes. Significant variability across ensemble member notwithstanding, one can still pick out overall lower amplitudes in the southern hemisphere for Cycle 25, and slightly delayed cycle onset of the northern hemisphere.



the southern hemisphere. Harder to pick out visually on Figure 3 but emerging from the quantitative analysis to be discussed presently, cycle onset in the northern hemisphere is also delayed by nearly 6 months with respect to onset in the southern hemisphere. This level of hemispheric asymmetry is well within the range typically produced by the LC17 model operating in dynamo mode (for more on this see Nagy, Lemerle, and Charbonneau, 2019).

Table 1 collects a number of metrics that can be extracted from our ensemble forecasts, namely: amplitude and date of peak ISSN in Cycle 25; date for onset of Cycle 25; and



**Table 1** Global and hemispheric forecasts for Cycle 25.

Metric	Global	N-hemisphere	S-hemisphere
Onset date	2020.49 <sup>+0.13</sup> <sub>-0.12</sub>	2021.00 <sup>+1.14</sup> <sub>-0.13</sub>	2020.49 <sup>+0.13</sup> <sub>-0.75</sub>
Peak ISSN	89 <sup>+29</sup> <sub>-14</sub>	50 <sup>+20</sup> <sub>-10</sub>	42 <sup>+16</sup> <sub>-9</sub>
Date of peak ISSN	2025.27 <sup>+0.89</sup> <sub>-1.05</sub>	2025.02 <sup>+1.14</sup> <sub>-0.93</sub>	2025.15 <sup>+1.13</sup> <sub>-1.39</sub>
Cycle duration	10.0 ± 0.74	10.2 ± 1.22	10.3 ± 1.44

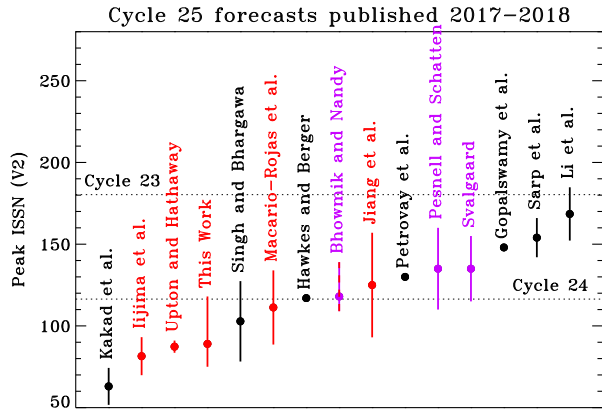
expected duration of Cycle 25. These quantities are given for the whole solar surface (second column), or separately for the northern and southern hemispheres (third and fourth columns). Working off the 13-month smoothed time series of monthly surface unsigned magnetic flux, the quoted figures and associated error ranges are constructed by ranking all corresponding measures in the 100-member ensemble, using the median as the prediction, and the 15% and 85% points of the ranked values as  $\pm$  uncertainly estimates. These are then converted into ISSN according to Equation 1. Cycle onset dates are set as the first appearance of Cycle 25 active regions in each ensemble member, and then ranked chronologically. The median is chosen as the predicted onset date, with the  $\pm$  ranges given in Table 1 spanning again the 15–85% range of these ranked dates. Cycle durations are defined as the time interval elapsed between appearance of the last Cycle 24 active region and last Cycle 25 active region, now simply averaged over the ensemble. Error estimates on Cycle durations are  $\pm$  one standard deviations about this mean.

Our forecasts for global and hemispheric cycle durations are notably smaller than the mean cycle period of 10.7 yr for the Cycle 21-calibrated reference solution of LC17. The dynamo model being kinematic, the meridional flow speed is fixed and the relatively short duration of our forecast Cycle 25 simply reflects the low magnetic amplitude of data-driven Cycle 24. The latter's internal magnetic toroidal component is weaker than average for the LC17 reference solution, and thus more easily reversed by the growing magnetic field of Cycle 25, leading to a duration shorter than an average cycle by half a year, for a majority of ensemble members. This difference is well within the duration spread of the LC17 model operating in dynamo mode (see Figure 8e in LC17).

Because our forecast is based on a dynamo model, it is possible in principle to extend the forecast beyond one cycle. However, the strong stochastic variability associated primarily with the scatter in the tilt angles of bipolar active regions effectively restricts the window for useful prediction to approximately one cycle (see Figure 2 in Nagy *et al.*, 2017). Examination of Figure 1 reveals that if these simulations were to be pushed beyond the end of Cycle 24, the onset of simulated Cycle 25 would take place very early for many ensemble members; such a two-cycle forecast of Cycle 25 would yield a very shallow minimum, a consequence of strong overlap between simulated Cycles 24 and 25, and a Cycle 25 peak amplitude much higher than our actual forecast based on the simulations plotted on Figure 2. This apparent internal inconsistency is associated with the fact that proper reproduction of the fairly rapid rise of Cycle 24 requires a relatively low internal magnetic field threshold value and relatively high dynamo number. This also leads to an early onset of Cycle 26 when pushing the ensemble simulations of Figure 2 beyond the end of Cycle 25. Despite a very wide range of forecasts, it remains noteworthy that the median-peak ISSN forecast for Cycle 26,  $215^{+179}_{-69}$  is back at the ISSN level of Cycle 23. Taken at face value, this result suggests that the announcement of a new Grand Minimum following Cycle 25 (Zharkova *et al.*, 2015) should be contemplated with due caution.



**Figure 4** A sample of recently published forecast for the peak ISSN amplitude (13-month smoothed monthly ISSN) for Cycle 25. The horizontal dotted lines indicate the peak smoothed ISSN values for Cycles 23 and 24, as labeled. Predictions in red are made using surface flux transport and/or dynamo models; predictions in purple are made using dynamo-based precursor methods. Forecasts in black collect other techniques.



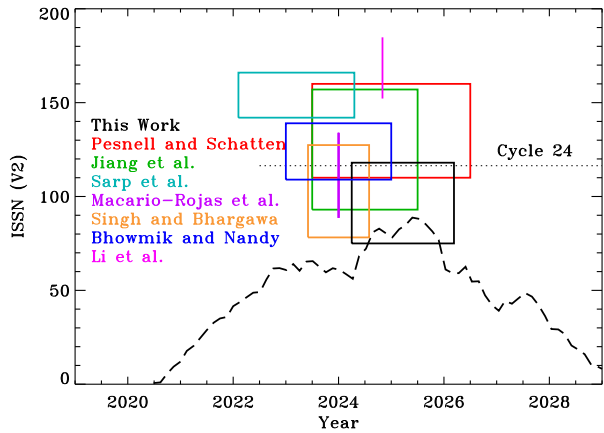
### 5. Comparison to Other Cycle 25 Forecasts

A number of forecasts based on various techniques have been published recently for the peak ISSN of Cycle 25 (e.g., Iijima *et al.*, 2017; Kakad, Kakad, and Ramesh, 2017; Singh and Bhargawa, 2017; Bhowmik and Nandy, 2018; Gopalswamy *et al.*, 2018; Hawkes and Berger, 2018; Jiang *et al.*, 2018; Li *et al.*, 2018; Macario-Rojas, Smith, and Roberts, 2018; Pesnell and Schatten, 2018; Petrovay *et al.*, 2018; Sarp *et al.*, 2018; Upton and Hathaway, 2018). Figure 4 summarizes pictorially these various forecasts, sorted from lowest to highest forecast peak ISSN amplitude, and including error estimates as stated by each set of authors.<sup>4</sup> This is by no means comprehensive, as we have restricted our selection to recent forecasts (published 2017–2018), but we did attempt to include all available forecasts based on dynamo or surface flux transport simulations, as well as precursor methods based on direct measurements of the solar surface dipole.

Our amplitude prediction is in the lower tier of these published forecasts, although its confidence interval spans almost the whole lower half of all compiled forecasts, a reflection of the large error estimates characterizing most forecasting methods. Nonetheless, even though the spread of this compilation is substantial, it remains much smaller than the corresponding spread of Cycle 24 forecasts compiled by Pesnell (2012) (see his Figure 3; note that his pre-2015 ISSN must be multiplied by a factor 1.45 for conversion to version 2 ISSN). Also noteworthy, our confidence interval spans all but one of the other forecasts based explicitly on surface flux transport models (Iijima *et al.*, 2017; Upton and Hathaway, 2018; Jiang *et al.*, 2018) or dynamo models (Macario-Rojas, Smith, and Roberts, 2018). Forecasts directly or indirectly based on the surface dipole as precursor (Bhowmik and Nandy, 2018; Pesnell and Schatten, 2018, and the Svalgaard forecast) also agree with each other within their stated error bar, but as a group stand significantly higher than the SFT-based forecasts, with the exception of Jiang *et al.* (2018); this is an interesting situation, as it suggests that we are likely to learn a lot from Cycle 25.

<sup>4</sup>The forecasts of Iijima *et al.* (2017) and Upton and Hathaway (2018) are not explicitly for the ISSN, but rather for the dipole at the end of Cycle 24. Here this (and the associated error estimate) is converted to ISSN by assuming that the ratio of Cycle 24/25 ISSN is the same as the ratio of dipole strength at the minimum preceding each cycle, as these authors themselves do to estimate the Cycle 25 amplitude. Gopalswamy *et al.* (2018), Hawkes and Berger (2018), and Petrovay *et al.* (2018) do not include a quantitative error estimate with their forecasts. The Svalgaard forecast is from a presentation at the March 2018 SORCE-TSIS Sun-Climate Symposium, and is as yet unpublished but is included here with permission.

**Figure 5** A sample of recently published forecast for the timing of peak ISSN amplitude (13-month smoothed monthly ISSN) for Cycle 25. The boxes draw span the quoted uncertainties in amplitude and peak time. The time series for the median of our ensemble is also replotted from Figure 2, rescaled to v2 ISSN using Equation 1.



A subset of the forecasts included on Figure 4 also include timing information for peak ISSN, ranging from  $2023 \pm 1.1$  (Sarp *et al.*, 2018) to  $2025 \pm 1.5$  (Pesnell and Schatten, 2018). Figure 5 displays these as error boxes spanning the quoted uncertainties in amplitude and timing (when provided), together with the median-rank time series of Figure 2. While the boxes can be quite large, most of these forecasts agree on a slow rising phase and (relatively) late epoch for Cycle 25 maximum.

Of the forecasts compiled on Figure 4, only Gopalswamy *et al.* (2018) gives hemispheric forecasts, namely S-ISSN = 89 and N-ISSN = 59; while this *level* of asymmetry is comparable to that predicted by our model, the asymmetry we predict is opposite, being characterized by a larger amplitude in the northern hemisphere (*cf.* Table 1). This highlights the potential of hemispheric measures as a discriminant of solar cycle forecasting methods.

## 6. Discussion and Conclusion

In this paper we have presented a detailed forecast for solar activity Cycle 25, based on a data-driven version of the solar cycle dynamo model of Lemerle and Charbonneau (2017). Our ensemble forecast predicts a Cycle 25 peak amplitude some 20% smaller than Cycle 24, corresponding to a version 2 ISSN  $89_{-14}^{+29}$  (13-month smoothed monthly values). Cycle 25 is predicted to show significant hemispheric asymmetries, with the S-hemisphere reaching peak ISSN values only 84% that of the peak N-hemisphere ISSN, but with cycle onset preceding the northern hemisphere by 6 months. Our forecast also suggests that despite its low amplitude and slow rise, Cycle 25 will be a relatively short cycle, with mean forecast duration  $10.0 \pm 0.74$  yr. In this respect our forecast Cycle 25 is morphologically similar to Solar Cycle 16, which showed a long rise time of 4.7 yr but a total duration of only 10.1 yr.

The direct output of our model are time series of unsigned magnetic flux associated with synthetic emerging active regions. This is of course very different from the international sunspot number (ISSN), which is defined as a weighted sum of sunspot groups and individual spots (Clette *et al.*, 2014). Conversion from our unsigned flux to an equivalent of the ISSN is carried out by a linear regression based on data from Cycle 23 and 24, namely Equation 1. It is far from clear that the same correlation should hold for cycles of varying amplitudes. This potential pitfall is not unique to our approach, as all other forecasting schemes must make similar assumptions regarding statistical stationarity.

Error estimates on our cycle forecast and associated time series reflect only the impact of stochasticity in active region emergence properties. While it has been argued that this is indeed the primary driver of cycle-to-cycle amplitude variability (Jiang, Cameron, and Schüssler, 2014; Karak and Miesch, 2017; Nagy *et al.*, 2017; Whitbread, Yeates, and Muñoz-Jaramillo, 2018), our dynamo model-based predictions are also subject to systematic errors associated with shortcomings of the dynamo model itself.

One obvious weakness of the LC17 dynamo models stems from its kinematic formulation: the large-scale flow fields, differential rotation and meridional circulation, in both the surface and internal modules, are considered given. Magnetographic data assimilation in surface flux transport models has shown that variations of the surface meridional flow can have a significant impact on the buildup of the surface dipole (Jiang *et al.*, 2010; Hathaway and Upton, 2016). This is an obvious needed improvement of the model. We are currently incorporating a generalization of the procedure introduced by Jiang *et al.* (2010) to model the collective effects of observed inflows towards active regions on the azimuthally averaged surface meridional flow in the surface module of the LC17 model (Nagy *et al.*, in prep). Preliminary results obtained thus far indicate that this feedback process tends to stabilize and slightly decrease the cycle amplitude, yet its overall impact across a given cycle appears milder than that associated with tilt angle fluctuations, or the emergence of a single “rogue” active region, especially when emerging close to the equator.

The meridional flow profile used in the LC17 model is characterized by a single-cell per meridional quadrant. This is also a likely source of systematic error, as helioseismic inversions suggest a more complex pattern (see, *e.g.* Zhao *et al.*, 2013; Rajaguru and Antia, 2015). However, we do note from the work of Hazra, Karak, and Choudhuri (2014) that from the dynamo point of view the key element is the presence of an equatorward flow at the base of the convection zone, still beyond the reach of helioseismic inversions of the internal meridional flow. Moreover, the latitudinal profile of the surface poleward flow yielding the best fit to synoptic magnetogram (Lemerle, Charbonneau, and Carignan-Dugas, 2015) differs slightly but significantly from the best-fit solar dynamo solution in LC17. A formal inversion of the internal meridional flow by genetic forward modeling (Charbonneau *et al.*, 1998), constrained by both synoptic magnetograms and the sunspot butterfly diagram, is an avenue we plan to explore.

Another potentially important source of systematic errors is associated with the use of two distinct databases for active region properties: when running in dynamo mode, the models draws active regions parameters from statistical distributions constructed from the database assembled by Wang and Sheeley (1989) for Cycle 21, while the data being assimilated beforehand pertains to Cycles 23 and/or 24. Numerous studies have highlighted small but significant cycle-to-cycle differences in active region properties (Dasi-Espuig *et al.*, 2010; McClintock and Norton, 2013; Tlatova *et al.*, 2018). Moreover, the data sources and reduction procedure used by Yeates, Mackay, and van Ballegoijen (2007) to generate their Cycle 23 and 24 active region database are also distinct from those used by Wang & Sheeley for Cycle 21, and thus likely subject to different detection threshold, selection biases, etc. While the two databases show significant differences in their distributions of various active region parameters, notably unsigned flux, we have verified that their flux-weighted distributions of tilt angles are quite similar; this being the primary determinant of dipole buildup (see, *e.g.*, Nagy *et al.*, 2017), one can hope that the resulting global dynamo behavior should not be too dissimilar. An obvious next step in testing and validating our forecast would be to repeat the formal optimization procedure carried out in LC17, but this time constraining the fit over Cycles 23 and 24, with an emergence function reflecting the statistical properties of the Yeates, Mackay, and van Ballegoijen (2007) active region database.

Our exploration of parameter space have also revealed a high sensitivity of the predicted Cycle 25 properties to the adopted threshold value ( $B^*$ ) on the internal toroidal field strength above which active region emergence takes place. Indeed, various combinations of this threshold value and dynamo number ( $K$ ) can provide equally acceptable reproductions of Cycle 24 unsigned flux time series upon assimilating active regions through Cycle 23 (*viz.* Figure 1). However, many of these parameter pairs, especially for low emergence threshold values, lead to active region emergences at mid-latitudes to high latitudes in the butterfly diagram. This non-solar behavior then justifies culling these solutions from our pool of acceptable solutions. The final adopted value  $B^* = 20$  is comfortably within the range allowed by the LC17 formal optimization procedure (see their Figure 2). With a dynamo number  $K = 1.7$ , our “best” predictive solution (Figure 2) operates rather close to criticality; increasing the threshold by a factor of 2, or reducing the dynamo number by as little as 25%, leads to a very weak Cycle 25, and no Cycle 26 for most of the ensemble members.

There is now ample observational and theoretical evidence that emergence of large active regions with unusual properties – notably strong deviation from Joy’s law – can derail the normal buildup of the solar surface dipole. Indeed the appearance of a few such “rogues” active regions in the descending phase of Cycle 23 has been invoked by Jiang, Cameron, and Schüssler (2015) as being responsible for the low amplitude of Cycle 24 (see also Whitbread, Yeates, and Muñoz-Jaramillo, 2018). The dynamo simulations reported upon in Nagy *et al.* (2017), also using the LC17 model, offer specific examples (see their §4) in which a single rogue active region emerging in the descending phase of the cycle can, depending on its tilt pattern, either derail the buildup of the solar dipole and shut down the cycle (their Figure 3), or kickstart a dying cycle back to normal cyclic behavior (their Figure 4). Again when taken at face value, these simulation results indicate that the fate of Cycle 25 will not be set until the last active region of Cycle 24 has emerged. At this writing, three active regions emerging with the expected Cycle 25 magnetic polarity pattern have been observed at high latitudes, but emergence of Cycle 24 regions at low heliographic latitude remains possible.

**Acknowledgements** We wish to express our gratitude to A. Yeates et A. Muñoz-Jaramillo for producing and maintaining their publicly available Cycle 23–24 active region database, again to A. Muñoz-Jaramillo for very useful discussions, and to an anonymous referee for some useful comments and suggestions. This work was supported by the Discovery Grant Program of Canada’s Natural Science and Engineering Research Council.

**Conflict of interest** The authors declare that they have no conflict of interest.

**Publisher’s Note** Springer Nature remains neutral with regard to jurisdictional claims in published maps and institutional affiliations.

## References

- Bhowmik, P., Nandy, D.: 2018, Prediction of the strength and timing of sunspot cycle 25 reveals decadal-scale space environmental conditions. *Nat. Commun.* **9**, 5209. DOI. ADS.
- Cameron, R.H., Jiang, J., Schüssler, M., Gizon, L.: 2014, Physical causes of solar cycle amplitude variability. *J. Geophys. Res.* **119**, 680. DOI. ADS.
- Charbonneau, P.: 2014, Solar dynamo theory. *Annu. Rev. Astron. Astrophys.* **52**, 251. DOI. ADS.
- Charbonneau, P., Tomczyk, S., Schou, J., Thompson, M.J.: 1998, The rotation of the solar core inferred by genetic forward modeling. *Astrophys. J.* **496**, 1015. DOI. ADS.
- Choudhuri, A.R., Chatterjee, P., Jiang, J.: 2007, Predicting solar cycle 24 with a solar dynamo model. *Phys. Rev. Lett.* **98**(13), 131103. DOI. ADS.

- Clette, F., Lefèvre, L.: 2016, The new sunspot number: assembling all corrections. *Solar Phys.* **291**, 2629. DOI. ADS.
- Clette, F., Svalgaard, L., Vaquero, J.M., Cliver, E.W.: 2014, Revisiting the sunspot number. a 400-year perspective on the solar cycle. *Space Sci. Rev.* **186**, 35. DOI. ADS.
- Dasi-Espuig, M., Solanki, S.K., Krivova, N.A., Cameron, R., Peñuela, T.: 2010, Sunspot group tilt angles and the strength of the solar cycle. *Astron. Astrophys.* **518**, A7. DOI. ADS.
- Dikpati, M., Charbonneau, P.: 1999, A Babcock–Leighton flux transport dynamo with solar-like differential rotation. *Astrophys. J.* **518**, 508. DOI. ADS.
- Dikpati, M., de Toma, G., Gilman, P.A.: 2006, Predicting the strength of solar cycle 24 using a flux-transport dynamo-based tool. *Geophys. Res. Lett.* **33**, L05102. DOI. ADS.
- Fan, Y.: 2009, Magnetic fields in the solar convection zone. *Living Rev. Solar Phys.* **6**, 4. DOI. ADS.
- Gopalswamy, N., Mäkelä, P., Yashiro, S., Akiyama, S.: 2018, Long-term solar activity studies using microwave imaging observations and prediction for cycle 25. *J. Atmos. Solar-Terr. Phys.* **176**, 26. DOI. ADS.
- Hathaway, D.H., Upton, L.A.: 2016, Predicting the amplitude and hemispheric asymmetry of solar cycle 25 with surface flux transport. *J. Geophys. Res.* **121**, 10. DOI. ADS.
- Hawkes, G., Berger, M.A.: 2018, Magnetic helicity as a predictor of the solar cycle. *Solar Phys.* **293**, 109. DOI. ADS.
- Hazra, G., Karak, B.B., Choudhuri, A.R.: 2014, Is a deep one-cell meridional circulation essential for the flux transport solar dynamo? *Astrophys. J.* **782**, 93. DOI. ADS.
- Iijima, H., Hotta, H., Imada, S., Kusano, K., Shiota, D.: 2017, Improvement of solar-cycle prediction: plateau of solar axial dipole moment. *Astron. Astrophys.* **607**, L2. DOI. ADS.
- Jiang, J., Cameron, R.H., Schüssler, M.: 2014, Effects of the scatter in sunspot group tilt angles on the large-scale magnetic field at the solar surface. *Astrophys. J.* **791**, 5. DOI. ADS.
- Jiang, J., Cameron, R.H., Schüssler, M.: 2015, The cause of the weak solar cycle 24. *Astrophys. J. Lett.* **808**, L28. DOI. ADS.
- Jiang, J., İşik, E., Cameron, R.H., Schmitt, D., Schüssler, M.: 2010, The effect of activity-related meridional flow modulation on the strength of the solar polar magnetic field. *Astrophys. J.* **717**, 597. DOI. ADS.
- Jiang, J., Wang, J.-X., Jiao, Q.-R., Cao, J.-B.: 2018, Predictability of the solar cycle over one cycle. *Astrophys. J.* **863**, 159. DOI. ADS.
- Kakad, B., Kakad, A., Ramesh, D.S.: 2017, Shannon entropy-based prediction of solar cycle 25. *Solar Phys.* **292**, 95. DOI. ADS.
- Karak, B.B., Miesch, M.: 2017, Solar cycle variability induced by tilt angle scatter in a Babcock–Leighton solar dynamo model. *Astrophys. J.* **847**, 69. DOI. ADS.
- Karak, B.B., Jiang, J., Miesch, M.S., Charbonneau, P., Choudhuri, A.R.: 2014, Flux transport dynamos: from kinematics to dynamics. *Space Sci. Rev.* **186**, 561. DOI. ADS.
- Lemerle, A., Charbonneau, P.: 2017, A coupled  $2 \times 2d$  Babcock–Leighton solar dynamo model. II. Reference dynamo solutions. *Astrophys. J.* **834**, 133. DOI. ADS.
- Lemerle, A., Charbonneau, P., Carignan-Dugas, A.: 2015, A coupled  $2 \times 2d$  Babcock–Leighton solar dynamo model. I. Surface magnetic flux evolution. *Astrophys. J.* **810**, 78. DOI. ADS.
- Li, F.Y., Kong, D.F., Xie, J.L., Xiang, N.B., Xu, J.C.: 2018, Solar cycle characteristics and their application in the prediction of cycle 25. *J. Atmos. Solar-Terr. Phys.* **181**, 110. DOI. ADS.
- Macario-Rojas, A., Smith, K.L., Roberts, P.C.E.: 2018, Solar activity simulation and forecast with a flux-transport dynamo. *Mon. Not. Roy. Astron. Soc.* **479**, 3791. DOI. ADS.
- McClintock, B.H., Norton, A.A.: 2013, Recovering Joy’s law as a function of solar cycle, hemisphere, and longitude. *Solar Phys.* **287**, 215. DOI. ADS.
- Muñoz-Jaramillo, A., Dasi-Espuig, M., Balmaceda, L.A., DeLuca, E.E.: 2013, Solar cycle propagation, memory, and prediction: insights from a century of magnetic proxies. *Astrophys. J. Lett.* **767**, L25. DOI. ADS.
- Nagy, M., Lemerle, A., Charbonneau, P.: 2019, Impact of rogue active regions on hemispheric asymmetry. *Adv. Space Res.* **63**, 1425. DOI. ADS.
- Nagy, M., Lemerle, A., Labonville, F., Petrovay, K., Charbonneau, P.: 2017, The effect of “rogue” active regions on the solar cycle. *Solar Phys.* **292**, 167. DOI. ADS.
- Pesnell, W.D.: 2012, Solar cycle predictions (invited review). *Solar Phys.* **281**, 507. DOI. ADS.
- Pesnell, W.D., Schatten, K.H.: 2018, An early prediction of the amplitude of solar cycle 25. *Solar Phys.* **293**, 112. DOI. ADS.
- Petrovay, K.: 2010, Solar cycle prediction. *Living Rev. Solar Phys.* **7**, 6. DOI. ADS.
- Petrovay, K., Nagy, M., Gerják, T., Juhász, L.: 2018, Precursors of an upcoming solar cycle at high latitudes from coronal green line data. *J. Atmos. Solar-Terr. Phys.* **176**, 15. DOI. ADS.
- Rajaguru, S.P., Antia, H.M.: 2015, Meridional circulation in the solar convection zone: time-distance helioseismic inferences from four years of HMI/SDO observations. *Astrophys. J.* **813**, 114. DOI. ADS.

- Sarp, V., Kilcik, A., Yurchyshyn, V., Rozelot, J.P., Ozguc, A.: 2018, Prediction of solar cycle 25: a non-linear approach. *Mon. Not. Roy. Astron. Soc.* **481**, 2981. DOI. ADS.
- Schatten, K.H., Scherrer, P.H., Svalgaard, L., Wilcox, J.M.: 1978, Using dynamo theory to predict the sunspot number during solar cycle 21. *Geophys. Res. Lett.* **5**, 411. DOI. ADS.
- Schüssler, M., Caligari, P., Ferriz-Mas, A., Moreno-Insertis, F.: 1994, Instability and eruption of magnetic flux tubes in the solar convection zone. *Astron. Astrophys.* **281**, L69. ADS.
- Singh, A.K., Bhargawa, A.: 2017, An early prediction of 25th solar cycle using Hurst exponent. *Astrophys. Space Sci.* **362**, 199. DOI. ADS.
- Svalgaard, L., Cliver, E.W., Kamide, Y.: 2005, Sunspot cycle 24: smallest cycle in 100 years? *Geophys. Res. Lett.* **32**, L01104. DOI. ADS.
- Tlatova, K., Tlatov, A., Pevtsov, A., Mursula, K., Vasil'eva, V., Heikkinen, E., Bertello, L., Pevtsov, A., Virtanen, I., Karachik, N.: 2018, Tilt of sunspot bipoles in solar Cycles 15 to 24. *Solar Phys.* **293**, 118. DOI. ADS.
- Upton, L.A., Hathaway, D.H.: 2018, An updated solar cycle 25 prediction with AFT: the modern minimum, arXiv e-prints. ADS.
- Wang, Y.-M., Sheeley, N.R. Jr.: 1989, Average properties of bipolar magnetic regions during sunspot cycle 21. *Solar Phys.* **124**, 81. DOI. ADS.
- Whitbread, T., Yeates, A.R., Muñoz-Jaramillo, A.: 2018, How many active regions are necessary to predict the solar dipole moment? *Astrophys. J.* **863**, 116. DOI. ADS.
- Yeates, A.R., Mackay, D.H., van Ballegoijen, A.A.: 2007, Modelling the global solar corona: filament chirality observations and surface simulations. *Solar Phys.* **245**, 87. DOI. ADS.
- Yeates, A.R., Nandy, D., Mackay, D.H.: 2008, Exploring the physical basis of solar cycle predictions: flux transport dynamics and persistence of memory in advection-versus diffusion-dominated solar convection zones. *Astrophys. J.* **673**, 544. DOI. ADS.
- Zhao, J., Bogart, R.S., Kosovichev, A.G., Duvall, T.L. Jr., Hartlep, T.: 2013, Detection of equatorward meridional flow and evidence of double-cell meridional circulation inside the Sun. *Astrophys. J. Lett.* **774**, L29. DOI. ADS.
- Zharkova, V.V., Shepherd, S.J., Popova, E., Zharkov, S.I.: 2015, Heartbeat of the Sun from principal component analysis and prediction of solar activity on a millennium timescale. *Sci. Rep.* **5**, 15689. DOI. ADS.